



# Pōniuā‘ena: A Luminous $z = 7.5$ Quasar Hosting a 1.5 Billion Solar Mass Black Hole

Jinyi Yang<sup>1</sup>, Feige Wang<sup>1,13</sup>, Xiaohui Fan<sup>1</sup>, Joseph F. Hennawi<sup>2,3</sup>, Frederick B. Davies<sup>2,4</sup>, Minghao Yue<sup>1</sup>, Eduardo Banados<sup>3</sup>, Xue-Bing Wu<sup>5,6</sup>, Bram Venemans<sup>3</sup>, Aaron J. Barth<sup>7</sup>, Fuyan Bian<sup>8</sup>, Konstantina Boutsia<sup>9</sup>, Roberto Decarli<sup>10</sup>, Emanuele Paolo Farina<sup>11</sup>, Richard Green<sup>1</sup>, Linhua Jiang<sup>5</sup>, Jiang-Tao Li<sup>12</sup>, Chiara Mazzucchelli<sup>8</sup>, and Fabian Walter<sup>3</sup>

<sup>1</sup> Steward Observatory, University of Arizona, 933 N. Cherry Avenue, Tucson, AZ 85721, USA; [jinyiyang@email.arizona.edu](mailto:jinyiyang@email.arizona.edu)

<sup>2</sup> Department of Physics, University of California, Santa Barbara, CA 93106-9530, USA

<sup>3</sup> Max Planck Institut für Astronomie, Königstuhl 17, D-69117 Heidelberg, Germany

<sup>4</sup> Lawrence Berkeley National Laboratory, 1 Cyclotron Road, Berkeley, CA 94720, USA

<sup>5</sup> Kavli Institute for Astronomy and Astrophysics, Peking University, Beijing 100871, People’s Republic of China

<sup>6</sup> Department of Astronomy, School of Physics, Peking University, Beijing 100871, People’s Republic of China

<sup>7</sup> Department of Physics and Astronomy, University of California, Irvine, CA 92697, USA

<sup>8</sup> European Southern Observatory, Alonso de Córdova 3107, Casilla 19001, Vitacura, Santiago 19, Chile

<sup>9</sup> Las Campanas Observatory, Carnegie Observatories, Colina El Pino, Casilla 601, La Serena, Chile

<sup>10</sup> INAF—Osservatorio di Astrofisica e Scienza dello Spazio di Bologna, via Gobetti 93/3, I-40129 Bologna, Italy

<sup>11</sup> Max Planck Institut für Astrophysik, Karl-Schwarzschild-Straße 1, D-85748 Garching bei München, Germany

<sup>12</sup> Department of Astronomy, University of Michigan, 311 West Hall, 1085 S. University Avenue, Ann Arbor, MI 48109-1107, USA

Received 2020 April 5; revised 2020 June 6; accepted 2020 June 9; published 2020 July 1

## Abstract

We report the discovery of a luminous quasar, J1007+2115 at  $z = 7.515$  (“Pōniuā‘ena”), from our wide-field reionization-era quasar survey. J1007+2115 is the second quasar now known at  $z > 7.5$ , deep into the reionization epoch. The quasar is powered by a  $(1.5 \pm 0.2) \times 10^9 M_\odot$  supermassive black hole (SMBH), based on its broad Mg II emission-line profile from Gemini and Keck near-IR spectroscopy. The SMBH in J1007+2115 is twice as massive as that in quasar J1342+0928 at  $z = 7.54$ , the current quasar redshift record holder. The existence of such a massive SMBH just 700 million years after the Big Bang significantly challenges models of the earliest SMBH growth. Model assumptions of Eddington-limited accretion and a radiative efficiency of 0.1 require a seed black hole of  $\gtrsim 10^4 M_\odot$  at  $z = 30$ . This requirement suggests either a massive black hole seed as a result of direct collapse or earlier periods of rapid black hole growth with hyper-Eddington accretion and/or a low radiative efficiency. We measure the damping wing signature imprinted by neutral hydrogen absorption in the intergalactic medium (IGM) on J1007+2115’s Ly $\alpha$  line profile, and find that it is weaker than that of J1342+0928 and two other  $z \gtrsim 7$  quasars. We estimate an IGM volume-averaged neutral fraction  $\langle x_{\text{H I}} \rangle = 0.39^{+0.22}_{-0.13}$ . This range of values suggests a patchy reionization history toward different IGM sightlines. We detect the 158  $\mu\text{m}$  [C II] emission line in J1007+2115 with the Atacama Large Millimeter/submillimeter Array; this line centroid yields a systemic redshift of  $z = 7.5149 \pm 0.0004$  and indicates a star formation rate of  $\sim 210 M_\odot \text{ yr}^{-1}$  in its host galaxy.

*Unified Astronomy Thesaurus concepts:* Quasars (1319); Intergalactic medium (813); Quasar absorption line spectroscopy (1317); Reionization (1383); Supermassive black holes (1663); Early universe (435)

## 1. Introduction

Luminous reionization-era quasars ( $z > 6.5$ ) provide unique probes of supermassive black hole (SMBH) growth, massive galaxy formation, and intergalactic medium (IGM) evolution in the first billion years of the universe’s history. However, efforts to find such objects have proven to be difficult because of a combination of the declining spatial density of quasars at high redshift, the limited sky coverage of near-infrared (NIR) photometry, and the low efficiency of spectroscopic follow-up observations.

During the past few years, high-redshift quasar searches using newly available wide-area optical and IR surveys have resulted in a sixfold increase in the number of known quasars at  $z > 6.5$ : 47 luminous quasars at  $z > 6.5$  have been discovered (e.g., Venemans et al. 2013, 2015; Mazzucchelli et al. 2017; Fan et al. 2019; Matsuoka et al. 2019a; Reed et al. 2019; Wang et al. 2019; Yang et al. 2019), although among them only 6 are at  $z \geq 7$  (Mortlock et al. 2011; Wang et al. 2018; Matsuoka et al. 2019a, 2019b; Yang et al. 2019) and one at  $z > 7.1$

(Bañados et al. 2018). These discoveries show that 800 million solar mass black holes exist already at  $z = 7.5$  (Bañados et al. 2018) and that the IGM is significantly neutral at  $z \gtrsim 7$  (e.g., Greig et al. 2017, 2019; Bañados et al. 2018; Davies et al. 2018b; Wang et al. 2020). However, both early SMBH growth history and IGM neutral fraction evolution at  $z > 7$  are still poorly constrained because of the small sample size. For statistical analysis, more  $z \sim 7$ –8 quasars are necessary to investigate the IGM, SMBH masses, and quasar host galaxies at this critical epoch.

In this Letter, we report the discovery of a new quasar J100758.264+211529.207 (“Pōniuā‘ena” in the Hawaiian language, hereinafter J1007+2115) at  $z = 7.5149$ . This object is only the second quasar known at  $z \sim 7.5$ , close to the midpoint redshift of reionization (Planck Collaboration et al. 2018). Its discovery enables new measurements of a quasar Ly $\alpha$  damping wing and provides new constraints on the earliest SMBH growth. In this Letter, we adopt a  $\Lambda$ CDM cosmology with parameters  $\Omega_\Lambda = 0.7$ ,  $\Omega_m = 0.3$ , and  $h = 0.685$ . Photometric data are reported on the AB system after applying a

<sup>13</sup> NHFP Hubble Fellow.

Galactic extinction correction (Schlegel et al. 1998; Schlafly & Finkbeiner 2011).

## 2. Candidate Selection and Observations

In this section we describe the selection method that led to the discovery of J1007+2115 and the spectroscopic observations. This quasar was selected based on the same photometric data set used for our previous  $z \sim 6.5$ –7 quasar surveys (Wang et al. 2018, 2019; Yang et al. 2019) but with selection criteria focused on a higher redshift range.

### 2.1. Selection Method

We have constructed an imaging data set by combining all available optical and infrared photometric surveys that cover  $\sim 20,000$  deg<sup>2</sup> of high Galactic latitude sky area with  $z/y$ ,  $J$ , and Wide-field Infrared Survey Explorer survey (WISE) photometry to the depth of  $J \sim 21$  ( $5\sigma$ ), and have used this data set to carry out a wide-field systematic survey for quasars at  $z > 6.5$  (Wang et al. 2018, 2019; Yang et al. 2019). J1007+2115 was selected in the area covered by the DESI Legacy Imaging Surveys (DECaLS; Dey et al. 2019), the Pan-STARRS1 (PS1; Chambers et al. 2016) survey, the UKIRT Hemisphere Survey (UHS; Dye et al. 2018), and WISE (Wright et al. 2010). For the WISE photometry, when we applied the selection cuts, we used the photometric data from the ALLWISE catalog.<sup>14</sup> To identify quasars at  $z \gtrsim 7.5$ , we required the object to be undetected in all optical bands. We used a simple IR color cut  $J - W1 > -0.261$ ,  $(S/N)_J > 5$ ,  $(S/N)_{W1} > 5$ . Forced aperture photometry in all PS1 and DECaLS bands was used to reject contaminants further. After the selection cuts, we visually inspected images of each candidate in all bands. In this step, both the ALLWISE and unWISE (Lang 2014; Meisner et al. 2018) images were included. All photometric data are summarized in Table 1.

### 2.2. Near-infrared Spectroscopy

J1007+2115 was confirmed as a quasar during our Gemini/Gemini Near-Infrared Spectrograph (GNIRS) run in 2019 May. The discovery spectrum was of low quality because of the high airmass when it was observed. A one-hour (on-source) observation with Magellan/Folded-port Infrared Echellette (FIRE) was used further to confirm this new quasar shortly after the GNIRS observations. To obtain higher quality spectra, we observed the quasar for 5.5 hr (on-source) with GNIRS and for 2.2 hr (on-source) with Keck/Near-Infrared Echellette Spectrometer (NIRES) in 2019 May and June. The redshift measured from the Mg II line is  $z_{\text{Mg II}} = 7.494 \pm 0.001$ . Since J1007+2115 was first discovered with the Gemini North Telescope in Hawaii, J1007+2115 was given the Hawaiian name “Pōniua’ena,” which means “unseen spinning source of creation, surrounded with brilliance” in the Hawaiian language.

With Gemini/GNIRS, we used the short-slit (cross-dispersion) mode ( $321 \text{ mm}^{-1}$ ) with simultaneous coverage of  $0.85$ – $2.5 \mu\text{m}$ . A  $1''.0$  slit ( $R \sim 400$ ) was used for the discovery observations, while a  $0''.675$  slit ( $R \sim 620$ ) was used for the additional high-quality spectrum. For Magellan/FIRE, the echelle mode with a  $0''.75$  slit ( $R \sim 4800$ ) was used. Keck/NIRES has a fixed configuration that simultaneously covers  $0.94$ – $2.45 \mu\text{m}$  with a fixed  $0''.55$  narrow slit resulting in a

<sup>14</sup> <http://wise2.ipac.caltech.edu/docs/release/allwise/>

**Table 1**  
Photometric Properties and Derived Parameters of J1007+2115

R.A. (J2000)	10:07:58.26
Decl. (J2000)	+21:15:29.20
$z_{[\text{C II}]}$	$7.5149 \pm 0.0004$
$m_{1450}$	$20.43 \pm 0.07$
$M_{1450}$	$-26.66 \pm 0.07$
$f_{\lambda,z\text{PS1}}^a$	$1.3 \times 10^{-18} \text{ erg s}^{-1} \text{ cm}^{-2} \text{ \AA}^{-1}$
$f_{\lambda,y\text{PS1}}^a$	$2.1 \times 10^{-18} \text{ erg s}^{-1} \text{ cm}^{-2} \text{ \AA}^{-1}$
$f_{\lambda,z\text{DECaLS}}^a$	$6.2 \times 10^{-19} \text{ erg s}^{-1} \text{ cm}^{-2} \text{ \AA}^{-1}$
$Y$	$21.30 \pm 0.13$
$J$	$20.20 \pm 0.18$
$H$	$20.00 \pm 0.07$
$K$	$19.75 \pm 0.08$
$W1$	$19.56 \pm 0.11$
$W2$	$19.44 \pm 0.20$
$z_{\text{Mg II}}$	$7.494 \pm 0.001$
$z_{\text{C IV}}$	$7.403 \pm 0.01$
$\alpha_\lambda$	$-1.14 \pm 0.01$
$\Delta v_{\text{Mg II}-[\text{C II}]}$	$-736 \pm 35 \text{ km s}^{-1}$
$\Delta v_{\text{C IV}-\text{Mg II}}$	$-3220 \pm 362 \text{ km s}^{-1}$
$\text{FWHM}_{\text{Mg II}}$	$3247 \pm 188 \text{ km s}^{-1}$
$\text{FWHM}_{\text{C IV}}$	$6821 \pm 2055 \text{ km s}^{-1}$
$\lambda L_{3000 \text{ \AA}}$	$(3.8 \pm 0.2) \times 10^{46} \text{ erg s}^{-1}$
$L_{\text{bol}}$	$(1.9 \pm 0.1) \times 10^{47} \text{ erg s}^{-1}$
$M_{\text{BH}}$	$(1.5 \pm 0.2) \times 10^9 M_\odot$
$L_{\text{bol}}/L_{\text{Edd}}$	$1.06 \pm 0.2$
$F_{[\text{C II}]}$	$1.2 \pm 0.1 \text{ Jy km s}^{-1}$
$\text{FWHM}_{[\text{C II}]}$	$331.3 \pm 31.6 \text{ km s}^{-1}$
$L_{[\text{C II}]}$	$(1.5 \pm 0.2) \times 10^9 L_\odot$
$S_{231.2 \text{ GHz}}$	$1.2 \pm 0.03 \text{ mJy}$
$\text{SFR}_{[\text{C II}]}$	$80\text{--}520 M_\odot \text{ yr}^{-1}$
$\text{SFR}_{\text{TIR}}$	$700 M_\odot \text{ yr}^{-1}$

#### Note.

<sup>a</sup> They are  $3\sigma$  flux limits in PS1  $z$ , PS1  $y$ , and DECaLS  $z$  bands, from our forced photometry with  $3''$  aperture diameter.

resolving power of  $R \sim 2700$  (Wilson et al. 2004). All NIR spectra were reduced with the open-source Python-based spectroscopic data reduction pipeline `PyPeIt`<sup>15</sup> (Prochaska et al. 2020). We corrected the telluric absorption by fitting an absorption model directly to the quasar spectra using the telluric model grids produced from the Line-By-Line Radiative Transfer Model (LBLRTM<sup>16</sup>; Clough et al. 2005). We stacked the spectra from GNIRS and NIRES, weighted by inverse variance, and scaled the result with the  $K$ -band magnitude. The final stacked spectrum is shown in Figure 1.

### 2.3. [C II]-based Redshift and Dust Continuum from ALMA

We observed J1007+2115 with the Atacama Large Millimeter/submillimeter Array (ALMA; configuration C43-4, Cycle 7) to detect the [C II] emission line and underlying dust continuum emission from the quasar host galaxy. The observations were taken in 2019 October with 15 minute on-source integration time. The synthesized beam size is  $0''.46 \times 0''.34$  and the final data cube reaches an rms noise level of  $0.4 \text{ mJy beam}^{-1}$  per  $10 \text{ km s}^{-1}$  channel. The ALMA

<sup>15</sup> <https://github.com/pypeit/PyPeIt>

<sup>16</sup> <http://rtweb.aer.com/lblrtm.html>

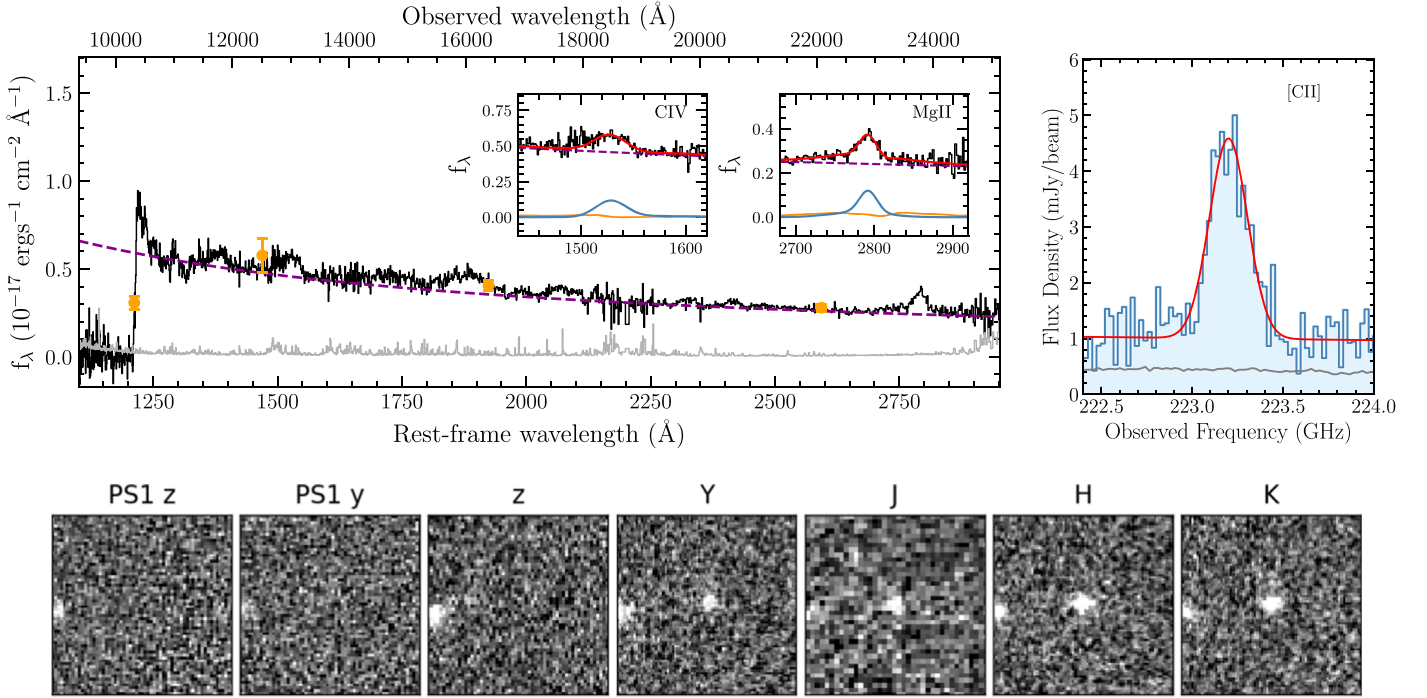


**Figure 1.** Upper left: the combined spectrum of J1007+2115 from GNIRS and NIRES data, compared with photometric data in the  $Y$ ,  $J$ ,  $H$ , and  $K$  bands (orange points with error bars). The  $J$ -band data point is from the UHS, and data in the other three bands are from our photometry with UKIRT obtained after the discovery of this quasar. The photometric data are consistent with the spectrum. The purple dashed line represents the best-fit pseudo-continuum. The two inner plots show the fits to the C IV and Mg II lines. The red solid lines represent the best-fit spectra. The orange lines are the Fe II components and the blue lines denote the best-fit emission lines. Upper right: the spectrum of the [C II] emission line with the uncertainty (gray) and best-fit Gaussian profile (red). The [C II] line peaks at the observed frequency  $223.2 \pm 0.01$  GHz, corresponding to a redshift of  $7.5149 \pm 0.0004$ . Bottom: images ( $15'' \times 15''$ , north is up and east is to the left) of J1007+2115 in PS1  $z$ , PS1  $y$ , DECaLS  $z$ , UKIRT  $Y$ , UHS  $J$ , UKIRT  $H$ , and UKIRT  $K$  bands. This quasar is not detected in PS1  $z$ , PS1  $y$ , and DECaLS  $z$ . The  $3\sigma$  flux limits in these three bands are measured from our forced photometry and reported in Table 1.

data were reduced with the CASA 5.4 pipeline (McMullin et al. 2007). J1007+2115 is strongly detected in both the [C II] emission line and the continuum. The source is not spatially resolved.

The [C II] emission line provides the most accurate measurement of the quasar systemic redshift. A Gaussian fit to the [C II] line yields a redshift of  $7.5149 \pm 0.0004$ . We use the [C II]-based redshift as the systemic redshift of the quasar. We obtain a line flux of  $F_{[\text{C II}]} = 1.2 \pm 0.1 \text{ Jy km s}^{-1}$ , and an FWHM of  $\text{FWHM}_{[\text{C II}]} = 331.3 \pm 31.6 \text{ km s}^{-1}$ , corresponding to a line luminosity of  $L_{[\text{C II}]} = (1.5 \pm 0.2) \times 10^9 L_{\odot}$ . Applying the relation between star formation rate (SFR)  $L_{[\text{C II}]}$  for high-redshift ( $z > 0.5$ ) galaxies from de Looze et al. (2014), which has a systematic uncertainty of a factor of  $\sim 2.5$ , we obtain  $\text{SFR}_{[\text{C II}]} \sim 80\text{--}520 M_{\odot} \text{ yr}^{-1}$ . This is similar to the SFR of quasar J1342+0928 at  $z = 7.54$  (Venemans et al. 2017). The underlying dust continuum is also detected, and we measure  $1.2 \pm 0.03 \text{ mJy}$  at 231.2 GHz. We obtain far-infrared (FIR: rest-frame  $42.5\text{--}122.5 \mu\text{m}$ ) and total infrared luminosities (TIR:  $8\text{--}1000 \mu\text{m}$ ) of  $L_{\text{FIR}} = (3.3 \pm 0.1) \times 10^{12} L_{\odot}$  and  $L_{\text{TIR}} = (4.7 \pm 0.1) \times 10^{12} L_{\odot}$ , assuming an optically thin graybody with dust temperature  $T_d = 47 \text{ K}$  and emissivity index  $\beta = 1.6$  (Beelen et al. 2006) and taking the effect of the cosmic microwave background on the dust emission into account (e.g., da Cunha et al. 2013). The  $\text{SFR}_{\text{TIR}}$  is estimated as  $\sim 700 M_{\odot} \text{ yr}^{-1}$  by applying the local scaling relation from Murphy et al. (2011).

### 3. A 1.5 Billion Solar Mass Black Hole

The central black hole mass of the quasar can be estimated based on its luminosity and the FWHM of the Mg II line. We fit the near-IR spectrum with a pseudo-continuum, including a power-law continuum, Fe II template (Vestergaard & Wilkes 2001; Tsuzuki et al. 2006), and Balmer continuum (de Rosa et al. 2014). Gaussian fits of the C IV and Mg II emission lines are performed on the continuum-subtracted spectrum. A two-component Gaussian profile is used. The uncertainty is estimated using 100 mock spectra created by randomly adding Gaussian noise at each pixel with its scale equal to the spectral error at that pixel (e.g., Shen et al. 2019; Wang et al. 2020). All uncertainties are then estimated based on the 16th and 84th percentiles of the distribution. The best-fit pseudo-continuum and the line fitting of C IV and Mg II are shown in Figure 1.

From the spectral fit, we find that the power-law continuum has a slope  $\alpha = -1.14 \pm 0.01$  ( $f_{\lambda} \propto \lambda^{\alpha}$ ). The rest-frame 3000 Å luminosity is measured to be  $\lambda L_{3000} = (3.8 \pm 0.2) \times 10^{46} \text{ erg s}^{-1}$ , corresponding to a bolometric luminosity of  $L_{\text{bol}} = (1.9 \pm 0.1) \times 10^{47} \text{ erg s}^{-1}$  assuming a bolometric correction factor of 5.15 (Richards et al. 2006). The apparent and absolute rest-frame 1450 Å magnitudes are derived to be  $m_{1450, \text{AB}} = 20.43 \pm 0.07$  and  $M_{1450, \text{AB}} = -26.66 \pm 0.07$  from the best-fit power-law continuum. The line fitting of Mg II yields an  $\text{FWHM} = 3247 \pm 188 \text{ km s}^{-1}$  and a Mg II-based redshift of  $z_{\text{Mg II}} = 7.494 \pm 0.001$ , implying a  $736 \pm 35 \text{ km s}^{-1}$  blueshift relative to the [C II] line, similar to other  $z \gtrsim 7$  luminous quasars (e.g., Mortlock et al. 2011; Bañados et al. 2018; Wang

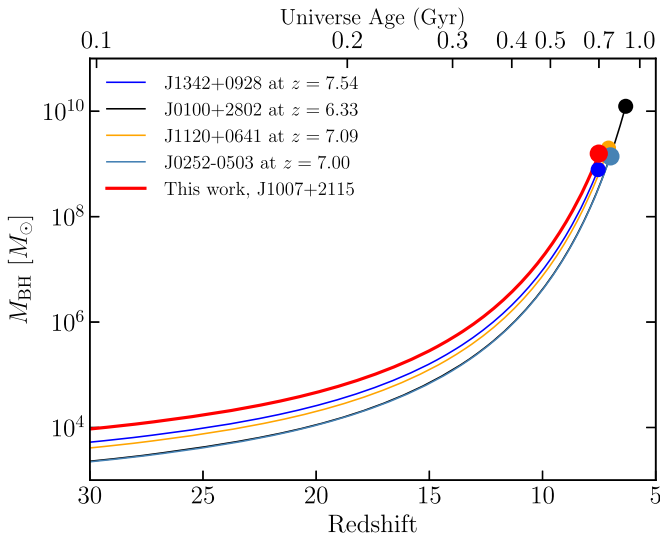


**Figure 2.** Black hole growth of J1007+2115, compared with those of quasars J1342+0928 at  $z = 7.54$  (Bañados et al. 2018), J1120+0641 at  $z = 7.09$  (Mortlock et al. 2011), J0252–0503 at  $z = 7.00$  (Wang et al. 2020), and J0100+2802 at  $z = 6.33$  (Wu et al. 2015). The black hole growth is modeled as  $M_{\text{BH}} = M_{\text{seed}} \exp[t/(0.05 \text{ Gyr})]$ , assuming that the black holes accrete at the Eddington limit with a radiative efficiency of 0.1 since seed formation. The curves are normalized to the observed black hole mass and redshift of these quasars. J1007+2115 requires the most massive seed black hole under the same assumptions of black hole growth.

et al. 2020). The C IV fitting results in an FWHM of  $6821 \pm 2055 \text{ km s}^{-1}$ . The C IV line has a  $3220 \pm 362 \text{ km s}^{-1}$  blueshift compared to the Mg II line. These measurements are summarized in Table 1.

We estimate the black mass based on the bolometric luminosity and the FWHM of the Mg II line by adopting the local empirical relation from Vestergaard & Osmer (2009). The black hole mass is derived to be  $M_{\text{BH}} = (1.5 \pm 0.2) \times 10^9 M_{\odot}$ , resulting in an Eddington ratio of  $L_{\text{bol}}/L_{\text{Edd}} = 1.1 \pm 0.2$ . Note that the black hole mass uncertainty estimated here does not include the systematic uncertainties of the scaling relation, which could be up to  $\sim 0.5$  dex. The uncertainty of the Eddington ratio is subject to the same systematic uncertainty as the black hole mass.

Observations of previously known luminous  $z \gtrsim 6.5$  quasars (e.g., Mortlock et al. 2011; Wu et al. 2015; Bañados et al. 2018) have already raised the question of how these early SMBHs grew in such a short time (e.g., Volonteri 2012; Smith et al. 2017; Inayoshi et al. 2019), which probably requires massive seed black holes, as illustrated in Figure 2. The black hole of J1007+2115, which is twice as massive as that of the other  $z = 7.5$  quasar J1342+0928, further exacerbates this early SMBH growth problem. To reach the observed SMBH mass at  $z = 7.5$ , a seed black hole with a mass of  $\sim 10^4$  (or  $3 \times 10^5$ )  $M_{\odot}$  would have to accrete continuously at the Eddington limit starting at  $z = 30$  (or 15), assuming a radiative efficiency of 0.1 (see Figure 2). Under this same set of fixed assumptions about black hole growth, J1007+2115 requires the most massive seed black hole compared to any other known quasar. This is consistent with the direct collapse black hole seed model rather than the Population III stellar remnant seed model. Even with a massive seed black hole, Eddington accretion with a high duty cycle and low radiative efficiency ( $\sim 0.1$ ) is required. A lower mass seed would imply an even higher accretion rate (e.g., hyper-Eddington accretion)

or a lower radiative efficiency (Davies et al. 2019). It has been suggested that maintaining super-Eddington accretion might be possible in specific environments (Inayoshi et al. 2016; Smith et al. 2017), but whether or not this mode of rapid black hole growth is sustainable remains an important open question.

#### 4. Constraint on the IGM Neutral Fraction from a Weak Damping Wing at $z = 7.5$

At  $z > 7$ , the damping wing profile, detectable as absorption redward of the Ly $\alpha$  emission line caused by the highly neutral IGM, is one of the most promising tracers of the IGM neutral fraction. J1007+2115 provides us with a new sightline to estimate the IGM neutral fraction through damping wing analysis at a time deep into the reionization epoch.

To estimate the IGM neutral fraction through damping wing analysis, we follow the procedures described in Davies et al. (2018a, 2018b), which has also been used to analyze the spectra of three other luminous  $z \gtrsim 7$  quasars (Davies et al. 2018a; Wang et al. 2020). Briefly, we first model the quasar intrinsic continuum around the Ly $\alpha$  region using the principal component analysis (PCA) approach in Davies et al. (2018b). This approach predicts the intrinsic blue-side quasar spectrum (rest-frame 1175–1280 Å) from the red-side spectrum (1280–2850 Å) using a training sample of  $\sim 13,000$  quasar spectra from the Sloan Digital Sky Survey / Baryon Oscillation Spectroscopic Survey (SDSS/BOSS) quasar catalog. We then apply the method from Davies et al. (2018a) to quantify the damping wing strength and estimate the volume-averaged neutral hydrogen fraction,  $\langle x_{\text{H I}} \rangle$ . This method models the quasar transmission spectrum with a multiscale hybrid model, which is a combination of the density, velocity, and temperature fields; large-scale semi-numerical reionization simulations around massive quasar-hosting halos (F. Davies & S. Furlanetto 2020, in preparation); and one-dimensional radiative transfer of ionizing photons emitted by the quasar (Davies et al. 2016). We construct realistic forward-modeled representations of quasar transmission spectra, accounting for the covariant intrinsic quasar continuum uncertainty. We then perform Bayesian parameter inference on the mock spectra to recover the joint posterior probability distribution functions (PDFs) of  $\langle x_{\text{H I}} \rangle$  and  $\log t_{\text{Q}}$  from the observed spectrum. In the Bayesian inference, the likelihood is computed from maximum pseudo-likelihood model parameters and the pseudo-likelihood is defined as the product of individual flux PDFs of  $500 \text{ km s}^{-1}$  binned pixels, equivalent to the likelihood function of the binned transmission spectrum in the absence of correlations between pixels (see more details in Davies et al. 2018a).

To measure  $\langle x_{\text{H I}} \rangle$ , we set a broad  $t_{\text{Q}}$  range of  $10^3 \text{ yr} < t_{\text{Q}} < 10^8 \text{ yr}$  with a flat log-uniform prior, and compute the posterior PDF of  $\langle x_{\text{H I}} \rangle$  by marginalizing over quasar lifetime. As shown in Figure 4, from the posterior PDF, we can estimate  $\langle x_{\text{H I}} \rangle$  and its 68% confidence interval as  $\langle x_{\text{H I}} \rangle = 0.39_{-0.13}^{+0.22}$ , which is consistent with the maximum pseudo-likelihood model parameters shown in Figure 3. To avoid possible contamination from any intervening damped Ly $\alpha$  absorber, we search for associated metal absorption. No such absorption has been found in our current spectrum. We conclude that the neutral IGM should be responsible for the damping wing features of J1007+2115. If any potential damped Ly $\alpha$  absorber plays a role in generating the damping wing feature, the IGM neutral fraction will be even lower.

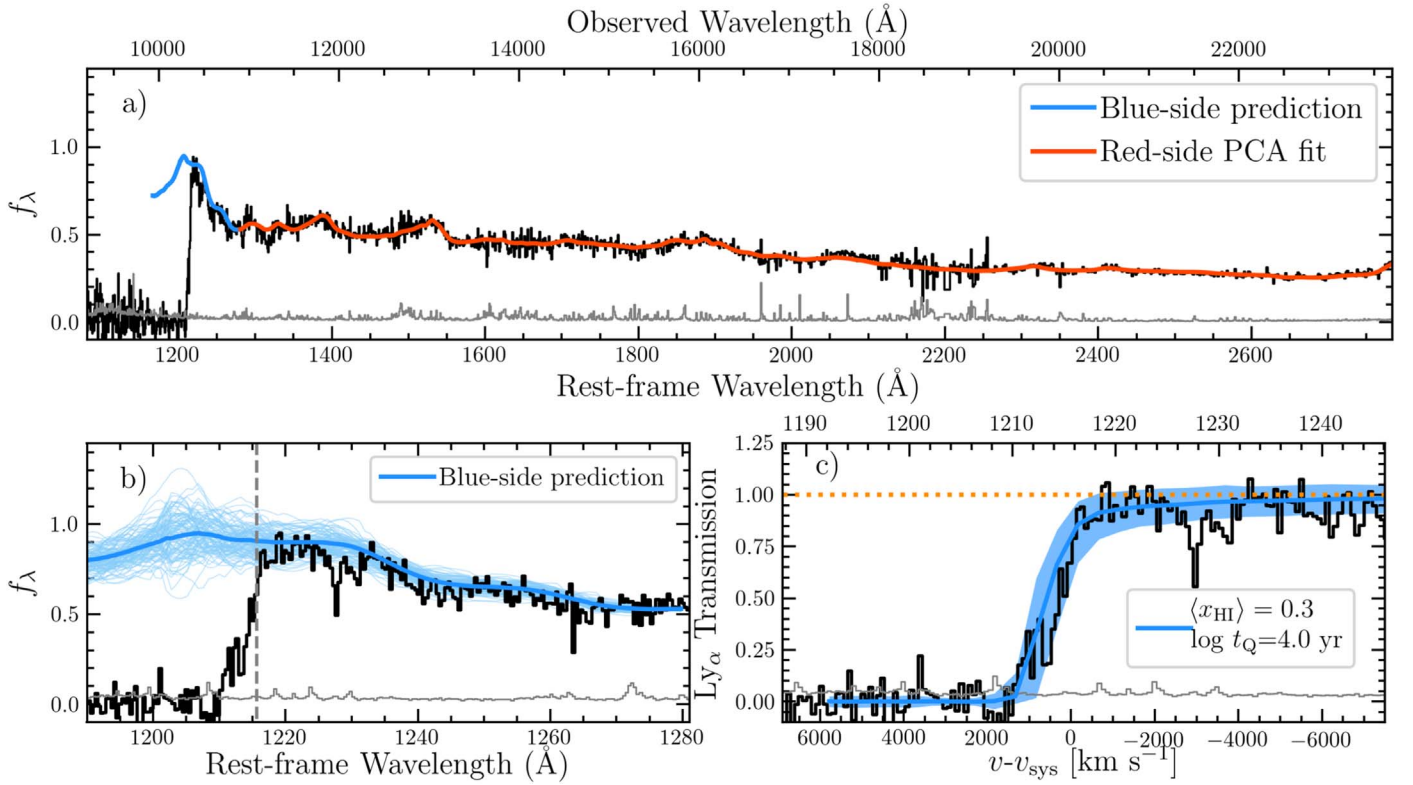


**Figure 3.** (a) Intrinsic quasar spectrum from our PCA fit (red-side) and prediction (blue-side), compared with the observed spectrum in Figure 1. (b) The zoom-in Ly $\alpha$  region with 100 draws (thinner blue lines) from the covariant prediction error calibrated from the 1% of most similar quasars in the PCA training sample. (c) The mock quasar transmission spectra with the volume-averaged neutral fraction  $\langle x_{\text{HI}} \rangle = 0.3$  and quasar lifetime  $t_Q = 10^{4.0}$  yr, which are from the maximum pseudo-likelihood model. The solid blue line represents the median of mock spectra and the shaded region is the the 16th–84th percentile range.

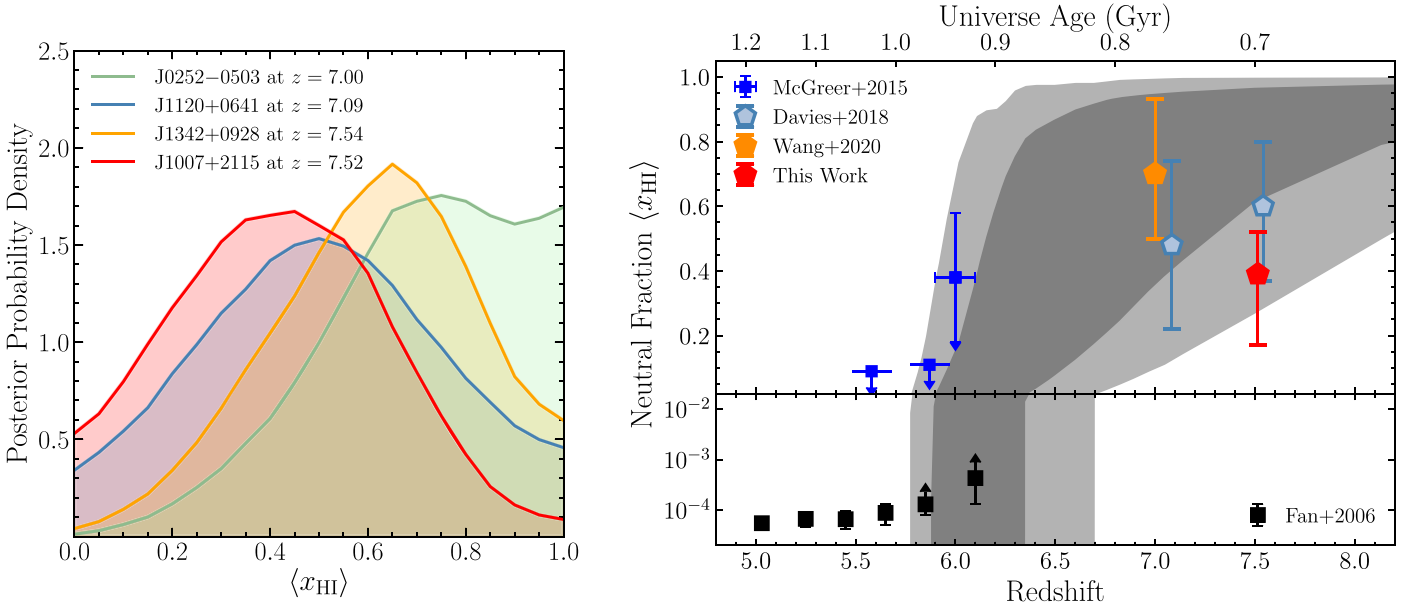


**Figure 4.** Left: the posterior PDF of the volume-averaged neutral fraction  $\langle x_{\text{HI}} \rangle$  for J1007+2115, compared to  $\langle x_{\text{HI}} \rangle$  estimated from the other  $z > 7$  quasars that show a damping wing (Davies et al. 2018a; Wang et al. 2020). Right: constraints on the IGM neutral fraction derived from high-redshift quasars through measurements of Ly $\alpha$  optical depth (Fan et al. 2006, black squares), dark gaps (McGreer et al. 2015, blue squares), and damping wings (Davies et al. 2018a; Wang et al. 2020, blue and orange pentagons). The new measurement for J1007+2115 is shown as the red filled pentagon. The dark and light gray shaded regions represent the 68% and 95% credible intervals from Planck observations (Planck Collaboration et al. 2018). These quasar measurements indicate a rapidly changing phase from  $z = 7.5$  to  $z = 6$  with large scatter in the neutral fraction.

The detection of damping wing signatures in two  $z > 7$  quasar spectra has previously provided strong evidence for a significantly neutral universe at  $z \gtrsim 7$  (e.g., Mortlock et al.

2011; Bañados et al. 2018; Davies et al. 2018a). Specifically, neutral gas fractions of  $\langle x_{\text{HI}} \rangle \sim 0.48$  at  $z = 7.09$  and  $\langle x_{\text{HI}} \rangle \sim 0.60$  at  $z = 7.54$  have been reported (Davies et al.

2018a). Recent analysis of the damping wing feature of the quasar J0252–0503 at  $z = 7.0$  (Wang et al. 2020) also suggests a highly neutral IGM with  $\langle x_{\text{H I}} \rangle = 0.7$ . All of these measurements are based on the same methodology used in this work. We compare our result with these estimates, as shown in Figure 4. It is evident that the damping wing absorption is much weaker in J1007+2115 compared to that in the other three  $z > 7$  quasars. At the resonant Ly $\alpha$  wavelength, the observed spectrum of J1007+2115 does not deviate from the blue-side prediction based on red-side PCA reconstruction. This result is to be compared with J0252–0503 (Wang et al. 2020) where the observed spectrum is  $\sim 40\%$  lower than the prediction without damping wing absorption. The  $\langle x_{\text{H I}} \rangle$  estimated from J1007+2115 at  $z = 7.54$  is lower than the measurements from all of the other three sightlines. Studies of the Ly $\alpha$  emission from  $z > 6$  galaxies have suggested neutral fractions of  $\langle x_{\text{H I}} \rangle = 0.59^{+0.11}_{-0.15}$  at  $z \sim 7$  and  $\langle x_{\text{H I}} \rangle > 0.76$  at  $z \sim 8$  (Mason et al. 2018, 2019). The sightline of J1007+2115 is thus a  $2\sigma$  outlier, compared to the previous results. Although it is difficult to draw solid conclusions because of the large uncertainties (and the broad PDF) on the value of  $\langle x_{\text{H I}} \rangle$ , the much weaker damping wing seen in J1007+2115’s spectrum indicates a significant scatter of the IGM neutral fraction in the redshift range  $z = 7.5$  to  $z = 7.0$ , which can be interpreted as observational evidence of patchy reionization.

## 5. Summary

We report the discovery of a new quasar J1007+2115 with a [C II]-based redshift of  $z = 7.5149 \pm 0.0004$ , selected with DECaLS, PS1, UHS, and WISE photometry and observed with the Gemini, Magellan, Keck, and ALMA telescopes. The [C II] and dust continuum emission from the quasar host galaxy are well detected, and imply an  $\text{SFR}_{[\text{C II}]} \sim 80\text{--}520 M_{\odot} \text{ yr}^{-1}$ . It is only the second quasar known at such high redshift and thus provides a valuable new data point for early SMBH and reionization history studies.

By fitting the NIR spectrum, we derive  $M_{\text{BH}} = (1.5 \pm 0.2) \times 10^9 M_{\odot}$  and an Eddington ratio of  $L_{\text{bol}}/L_{\text{Edd}} = 1.06 \pm 0.2$  using the broad Mg II emission line. The black hole in J1007+2115 is twice as massive as that of J1342+0928 at a very similar redshift of  $z = 7.54$ , and thus places the strongest constraint to the early SMBH growth, requiring a seed black hole with a mass of  $\sim 10^4 (3 \times 10^5) M_{\odot}$  at  $z = 30 (15)$ . Through damping wing modeling of the quasar spectrum, we estimate the volume-averaged neutral fraction to be  $\langle x_{\text{H I}} \rangle = 0.39^{+0.22}_{-0.13}$  at  $z = 7.5$ . Together with three previous measurements from quasar damping wing analyses, our new result indicates a large scatter of the IGM neutral fraction from  $z = 7.5$  to  $z = 7.0$ , indicative of a patchy reionization process.

Thanks to Dave Osip for approving the request of FIRE spectroscopy, which is important to the confirmation of this quasar. J.Y., X.F., and M.Y. acknowledge support from the NASA ADAP grant NNX17AF28G. F.W. thanks NASA for the support provided through the NASA Hubble Fellowship grant #HST-HF2-51448.001-A awarded by the Space Telescope Science Institute, which is operated by the Association of Universities for Research in Astronomy, Incorporated, under NASA contract NAS5-26555. L.J. and X.-B.W. thank the National Key R&D Program of China (2016YFA0400703) and the National Science Foundation of China (11533001 &

11721303) for their support. Research by A.J.B. is supported by NSF grant AST-1907290.

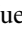
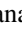
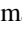
Some of the data presented in this Letter were obtained at the W.M. Keck Observatory, which is operated as a scientific partnership among the California Institute of Technology, the University of California and the National Aeronautics and Space Administration. The Observatory was made possible by the generous financial support of the W. M. Keck Foundation. The authors wish to recognize and acknowledge the very significant cultural role and reverence that the summit of Maunakea has always had within the indigenous Hawaiian community. We are most fortunate to have the opportunity to conduct observations from this mountain. This research is based in part on observations obtained at the Gemini Observatory (GN-2019B-Q-135, GN-2019A-DD-109), which is operated by the Association of Universities for Research in Astronomy, Inc., under a cooperative agreement with the NSF on behalf of the Gemini partnership: the National Science Foundation (United States), National Research Council (Canada), CONICYT (Chile), Ministerio de Ciencia, Tecnología e Innovación Productiva (Argentina), Ministério da Ciência, Tecnologia e Inovação (Brazil), and Korea Astronomy and Space Science Institute (Republic of Korea). This paper makes use of the following ALMA data: ADS/JAO.ALMA#2019.1.01025.S. ALMA is a partnership of ESO (representing its member states), NSF (USA) and NINS (Japan), together with NRC (Canada), MOST and ASIAA (Taiwan), and KASI (Republic of Korea), in cooperation with the Republic of Chile. The Joint ALMA Observatory is operated by ESO, AUI/NRAO and NAOJ. The National Radio Astronomy Observatory is a facility of the National Science Foundation operated under cooperative agreement by Associated Universities, Inc. UKIRT is owned by the University of Hawaii (UH) and operated by the UH Institute for Astronomy; operations are enabled through the cooperation of the East Asian Observatory. This paper includes data gathered with the 6.5 m Magellan Telescopes located at Las Campanas Observatory, Chile. We acknowledge the use of the PyPeIt data reduction package.











Thanks to the Leo Ola program for naming this quasar in Hawaiian language. The name Pōniuā’ena is a result of the Leo Ola program offered through the University of Hawai’i at Hilo’s Ka Haka ‘Ula o Ke‘elikōlani, College of Hawaiian Language and the ‘Imiloa Astronomy Center. The efforts undertaken through Leo Ola help to create a pathway where language and culture are at the core of modern scientific practices, melding indigenous culture and science locally, nationally, and worldwide.

*Facilities:* Gemini (GMOS), Keck (NIREs), Magellan (FIRE), UKIRT (WFCam), ALMA.

*Software:* PyPeIt (Prochaska et al. 2020).

## ORCID iDs

Jinyi Yang  <https://orcid.org/0000-0001-5287-4242>  
 Feige Wang  <https://orcid.org/0000-0002-7633-431X>  
 Xiaohui Fan  <https://orcid.org/0000-0003-3310-0131>  
 Joseph F. Hennawi  <https://orcid.org/0000-0002-7054-4332>  
 Frederick B. Davies  <https://orcid.org/0000-0003-0821-3644>  
 Minghao Yue  <https://orcid.org/0000-0002-5367-8021>  
 Eduardo Banados  <https://orcid.org/0000-0002-2931-7824>  
 Xue-Bing Wu  <https://orcid.org/0000-0002-7350-6913>  
 Bram Venemans  <https://orcid.org/0000-0001-9024-8322>

Aaron J. Barth  <https://orcid.org/0000-0002-3026-0562>  
 Fuyan Bian  <https://orcid.org/0000-0002-1620-0897>  
 Konstantina Boutsia  <https://orcid.org/0000-0003-4432-5037>  
 Roberto Decarli  <https://orcid.org/0000-0002-2662-8803>  
 Emanuele Paolo Farina  <https://orcid.org/0000-0002-6822-2254>  
 Richard Green  <https://orcid.org/0000-0003-1245-5232>  
 Linhua Jiang  <https://orcid.org/0000-0003-4176-6486>  
 Jiang-Tao Li  <https://orcid.org/0000-0001-6239-3821>  
 Chiara Mazzucchelli  <https://orcid.org/0000-0002-5941-5214>  
 Fabian Walter  <https://orcid.org/0000-0003-4793-7880>

## References

- Bañados, E., Venemans, B. P., Mazzucchelli, C., et al. 2018, *Natur*, **553**, 473  
 Beelen, A., Cox, P., Benford, D. J., et al. 2006, *ApJ*, **642**, 694  
 Chambers, K. C., Magnier, E. A., Metcalfe, N., et al. 2016, arXiv:1612.05560  
 Clough, S. A., Shephard, M. W., Mlawer, E. J., et al. 2005, *JQSRT*, **91**, 233  
 da Cunha, E., Groves, B., Walter, F., et al. 2013, *ApJ*, **766**, 13  
 Davies, F. B., Furlanetto, S. R., & McQuinn, M. 2016, *MNRAS*, **457**, 3006  
 Davies, F. B., Hennawi, J. F., Bañados, E., et al. 2018a, *ApJ*, **864**, 142  
 Davies, F. B., Hennawi, J. F., Bañados, E., et al. 2018b, *ApJ*, **864**, 143  
 Davies, F. B., Hennawi, J. F., & Eilers, A.-C. 2019, *ApJL*, **884**, L19  
 de Looze, I., Cormier, D., Leboutteiller, V., et al. 2014, *A&A*, **568**, A62  
 de Rosa, G., Venemans, B. P., Decarli, R., et al. 2014, *ApJ*, **790**, 145  
 Dey, A., Schlegel, D. J., Lang, D., et al. 2019, *AJ*, **157**, 168  
 Dye, S., Lawrence, A., Read, M. A., et al. 2018, *MNRAS*, **473**, 5113  
 Fan, X., Strauss, M. A., Becker, R. H., et al. 2006, *AJ*, **132**, 117  
 Fan, X., Wang, F., Yang, J., et al. 2019, *ApJL*, **870**, L11  
 Greig, B., Mesinger, A., & Bañados, E. 2019, *MNRAS*, **484**, 5094  
 Greig, B., Mesinger, A., Haiman, Z., & Simcoe, R. A. 2017, *MNRAS*, **466**, 4239  
 Inayoshi, K., Haiman, Z., & Ostriker, J. P. 2016, *MNRAS*, **459**, 3738  
 Inayoshi, K., Visbal, E., & Haiman, Z. 2019, arXiv:1911.05791  
 Lang, D. 2014, *AJ*, **147**, 108  
 Mason, C. A., Fontana, A., Treu, T., et al. 2019, *MNRAS*, **485**, 3947  
 Mason, C. A., Treu, T., Dijkstra, M., et al. 2018, *ApJ*, **856**, 2  
 Matsuoka, Y., Iwasawa, K., Onoue, M., et al. 2019a, *ApJ*, **883**, 183  
 Matsuoka, Y., Onoue, M., Kashikawa, N., et al. 2019b, *ApJL*, **872**, L2  
 Mazzucchelli, C., Bañados, E., Venemans, B. P., et al. 2017, *ApJ*, **849**, 91  
 McGreer, I. D., Mesinger, A., & D'Odorico, V. 2015, *MNRAS*, **447**, 499  
 McMullin, J. P., Waters, B., Schiebel, D., et al. 2007, in ASP Conf. Ser. 376, *Astronomical Data Analysis Software and Systems XVI*, ed. R. A. Shaw, F. Hill, & D. J. Bell (San Francisco, CA: ASP), 127  
 Meisner, A. M., Lang, D., & Schlegel, D. J. 2018, *RNAAS*, **2**, 1  
 Mortlock, D. J., Warren, S. J., Venemans, B. P., et al. 2011, *Natur*, **474**, 616  
 Murphy, E. J., Condon, J. J., Schinnerer, E., et al. 2011, *ApJ*, **737**, 67  
 Planck Collaboration, Aghanim, N., Akrami, Y., et al. 2018, arXiv:1807.06209  
 Prochaska, J. X., Hennawi, J., Cooke, R., et al. 2020, pypeit/PypeIt, v0.11.0, Zenodo, doi:10.5281/zenodo.3743493  
 Reed, S. L., Banerji, M., Becker, G. D., et al. 2019, *MNRAS*, **487**, 1874  
 Richards, G. T., Lacy, M., Storrie-Lombardi, L. J., et al. 2006, *ApJS*, **166**, 470  
 Schlafly, E. F., & Finkbeiner, D. P. 2011, *ApJ*, **737**, 103  
 Schlegel, D. J., Finkbeiner, D. P., & Davis, M. 1998, *ApJ*, **500**, 525  
 Shen, Y., Wu, J., Jiang, L., et al. 2019, *ApJ*, **873**, 35  
 Smith, A., Bromm, V., & Loeb, A. 2017, *A&G*, **58**, 3.22  
 Tsuzuki, Y., Kawara, K., Yoshii, Y., et al. 2006, *ApJ*, **650**, 57  
 Venemans, B. P., Bañados, E., Decarli, R., et al. 2015, *ApJL*, **801**, L11  
 Venemans, B. P., Findlay, J. R., Sutherland, W. J., et al. 2013, *ApJ*, **779**, 24  
 Venemans, B. P., Walter, F., Decarli, R., et al. 2017, *ApJL*, **851**, L8  
 Vestergaard, M., & Osmer, P. S. 2009, *ApJ*, **699**, 800  
 Vestergaard, M., & Wilkes, B. J. 2001, *ApJS*, **134**, 1  
 Volonteri, M. 2012, *Sci*, **337**, 544  
 Wang, F., Yang, J., Fan, X., et al. 2018, *ApJL*, **869**, L9  
 Wang, F., Yang, J., Fan, X., et al. 2019, *ApJ*, **884**, 30  
 Wang, F., Davies, F. B., Yang, J., et al. 2020, *ApJ*, **896**, 23  
 Wilson, J. C., Henderson, C. P., Herter, T. L., et al. 2004, *Proc. SPIE*, **5492**, 1295  
 Wright, E. L., Eisenhardt, P. R. M., Mainzer, A. K., et al. 2010, *AJ*, **140**, 1868  
 Wu, X.-B., Wang, F., Fan, X., et al. 2015, *Natur*, **518**, 512  
 Yang, J., Wang, F., Fan, X., et al. 2019, *AJ*, **157**, 236